Journal of Porous Media 10(7), 657–675 (2007)

Simulation of Melting of Ice under a Constant Temperature Heat Source Using a Combined Transfinite Interpolation and Partial Differential Equation Methods

P. Rattanadecho and C. Serttikul

Faculty of Engineering, Thammasat University (Rangsit Campus), Pathumthani 12121, Thailand

E-mail: ratphadu@engr.tu.ac.th

ABSTRACT

Within the framework of the novel numerical method, this article presents an efficient algorithm for solving multidimensional nonlinear heat problem involving phase change. A numerical study is made for melting of ice subjected to a constant temperature heat source with different initial conditions. The algorithmic design is based on two steps: Preliminary grids are first generated by an algebraic method, that is, a transfinite interpolation method, with subsequent refinement using a Partial Differential Equation (PDE) mapping (parabolic grid generation) method in the next step. Numerical examples are given for the two melting conditions: low and very low initial temperatures. The accuracy and flexibility of the presented numerical methods are verified by comparing the results with existing analytical solutions. The simulated results are also compared with the experimental results. In summary, the algorithm is able to efficiently and accurately predict the evolution of temperature distribution and deformation of an interface (melting front) with smooth grid point distribution. An important application of the present algorithm would be in the field of phase change problems.

Received March 17, 2006; Accepted October 2, 2006

NOMENCLATURE

a	thermal diffusivity (m^2/s)	λ	effective thermal conductivity (W/mK)
C_p	specific heat capacity (J/kgK)	**Subscripts**	
L	latent heat (J/kg)	i	initial
t	time (s)	f	fusion
T	temperature (°C)	l	unfrozen
x, z	Cartesian coordinates	s	frozen
Greek Symbols			

1. INTRODUCTION

Phase change problems (solidification or melting) are also known as Stefan problems or moving boundary problems. The solution of moving boundary problems with phase change has been of special interest due to the inherent difficulties associated with the nonlinearity of the interface conditions and the unknown locations of the arbitrary moving boundaries. Solidification and melting are important parts of manufacturing processes such as crystal growth, casting, welding, surface alloying, dip forming, coating process, latent heat storage, aerodynamic ablation, casting of metal, food processing, and production of printed circuit electronics. In all these processes, phase changes of material are caused by the heat transfer to and from both of the phases on either side of the interface. This yields melting if the net heat is added to the solid part of the interface, and solidification when the net heat is subtracted.

Owing to their importance, many numerical approximations have been developed to solve these problems (Landua, 1950; Murray and Landis, 1959; Frivik and Comini, 1982; Weaver and Viskanta, 1986; Chellaiah and Viskanta, 1988). This can be classified into two main categories: front tracking methods and fixed grid methods. With front tracking methods (Gupta, 2000; Pardo and Weckman, 1990; Voller et al., 1990; Gong and Mujumdar, 1998; Rattanadecho, 2004a, 2004b), the discrete phase change front is tracked continuously and treated as a moving boundary between the liquid and solid phases. In the mathematical formulation, two different sets of governing equations are solved in each of the phases. The Stefan boundary condition is used at the solid-liquid interface to calculate the interface velocity, and the interface is then moved, depending on this velocity, after each time step. The latent heat involved in the phase change is treated explicitly as an internal boundary condition. The change in size and shape of the computational domain requires either grid movement techniques or coordinate system transformations. Furthermore, the front tracking method is applicable for problems with isothermal phase changes. It is generally not suitable for problems where the phase change takes place within a temperature interval and involves the formation of a so-called mushy region. With fixed grid methods (Fachinotti et al., 1999; Morgan et al., 1978; Nedjar, 2002; Tamma and Namburu, 1990; Voller and Cross, 1981; Beckett et al., 2001, 2002; Cao et al., 1999; Mackenzie and Robertson, 2000; Tenchev et al., 2005), the phase change front is not tracked explicitly, but is instead recovered a posteriori from the computed temperature field. These methods are also known as single-domain methods because the

same differential equation can be used for the solid and liquid regions. These approaches are collectively known as the enthalpy method because they can be derived from the energy conservation equation written in terms of the enthalpy, which is the sum of the apparent and latent heat. Enthalpy methods are the natural choice when the phase change occurs over a temperature interval. In the case of isothermal phase change, there is a discontinuity in the enthalpy across the phase change front, which is normally smoothed by assuming that the phase change occurs over a temperature interval (Tenchev et al., 2005).

As mentioned above, the conventional numerical methods, that is, front tracking methods and fixed grid methods, have been widely used because of easy-to-handle numerical algorithms. However, in numerical approximations of these methods with discontinuous coefficients, often, the largest numerical errors are introduced in a neighborhood of the discontinuities. The troublesome numerical errors in conventional methods are effectively reduced if the grid generation and solution procedures are separate from the discontinuities, and special formulas are used to incorporate the jump conditions directly into the numerical model. Compared with the conventional methods, less effort has been put into computing the phase change problems with the concept of the separation of grid generation and the solution procedure, that is, the combined transfinite interpolation and the PDE mapping method. A combined transfinite interpolation and PDE mapping method leads to the achievement of a very smooth grid point distribution, and boundary point discontinuities are smoothed out in the interior domain. The idea behind the method is as follows. The first step is to create a computational grid in body-fitted coordinates, involving two basic steps: (1) define an origin point and (2) specify the distribution (number and spacing) of grid nodes along the edges of the geometric regions as well as the moving boundary between the liquid and solid phases. The automatic grid generator then takes over and, using an algebraic technique known as transfinite interpolation, creates a grid that simultaneously matches the edge node prescription and conforms to the irregular edges of the body-fitted geometry. Grid generation by algebraic methods produces high-quality numerical grids and allow for the very efficient integration of the thermal-flow field physics. Considering grid optimization, the designed grid optimization algorithm improves on the transfinite interpolation method by carrying the grid generation process one step further. In the final step, it uses an automatically generated grid as an initial approximation to a higher-quality grid system derived using the technique of PDE grid generation. This technique offers advantages over purely algebraic methods: (1) good control over the skewness and spacing of the derived grid on surface interiors, while simultaneously allowing complete control over the grid spacing (node distribution) on surface edges as well as on the moving boundary, and (2) an ability to produce unique, stable, and smooth grid distributions free of interior maxima or minima (inflection points) in body-fitted coordinates. PDE grid generation works well with irregularly shaped geometries and can produce grids that are highly conformal with the edges of individual computational surfaces. The means for grid generation should not be dictated by the limitations of a given specific field solution procedure, and conversely, the method that determines the field should accept as input an arbitrary set of coordinate points that constitutes the grid. Nevertheless, of course, these two operations can never be totally independent because the logistic structure of the information, the location of outer boundaries, the nature of the coordinates, and the types of grid singularities are items that have to be closely coordinated between the flow solver and the grid generator (Eriksson, 1982).

Grid generation for multidimensional geometries using transfinite interpolation functions was studied by Coons (1967), Cook (1974), and Gordon and Hall (1973). Ettouney and Brown (1983) successfully modeled slightly nonplanar interfaces by using an algebraic grid generation system, where the interface was described in terms of univariate function. Although

grid generation is the heart of most numerical algorithms for flow problems or non-phase-change problems, little effort has been reported on phase change problems, particularly the problem that couples the grid generation algorithm with the flow solution.

The present article introduces the novel numerical approach mentioned above, which extends the range of the initial and boundary conditions in the case of melting of ice subjected to a constant-temperature heat source that can be covered. It will also permit a continuous determination of the melting front movement and indicate the internal temperature distribution. It offers the highest overall accuracies and a smooth grid point distribution. Numerically, for generating a boundary/interface-fitted coordinate system, structured grids are initialized using the transfinite interpolation-algebraic method, and the quality of structured grids can be significantly improved by applying parabolic-PDE methods. These methods iteratively solve the unsteady conduction equation together with the moving boundary condition, considered to be conduction as the only mode of heat transfer in both the unfrozen and frozen layers.

2. MATHEMATICAL FORMULATION

The two-dimensional system illustrated schematically in Fig. 1 is considered. Initially, the walls are all insulated, and the rectangular cavity is filled with phase change material (PCM) in the solid state (ice) having the fusion temperature of T_f. A constant-temperature (T_H) heat source is applied at the bottom wall. At time $t = 0$, the melting process upwardly begins. The applicable differential equations for two-dimensional heat flow with constant thermal properties for the unfrozen and frozen layers are, respectively,

$$\frac{\partial T_l}{\partial t} = a_l \left(\frac{\partial^2 T_l}{\partial x^2} + \frac{\partial^2 T_l}{\partial z^2} \right) + \left(\frac{\partial T_l}{\partial z} \right) \frac{dz}{dt} \qquad (1)$$

$$\frac{\partial T_s}{\partial t} = a_s \left(\frac{\partial^2 T_s}{\partial x^2} + \frac{\partial^2 T_s}{\partial z^2} \right) + \left(\frac{\partial T_s}{\partial z} \right) \frac{dz}{dt} \qquad (2)$$

where the last terms of Eqs. (1) and (2) results from a coordinate transformation attached to the moving boundary. In the unfrozen layer, internal natural convection can be neglected because the melting process is fast.

Equations (1) and (2) are based on the following assumptions: (1) the temperature field can be assumed to be two-dimensional; (2) the thermal equilibrium exists between PCM and PM; this is possible when the porous matrix has a little larger thermal conductivity than the PCM, and the interphase heat transfer can be properly neglected; and (3) properties of PM are isotropic.

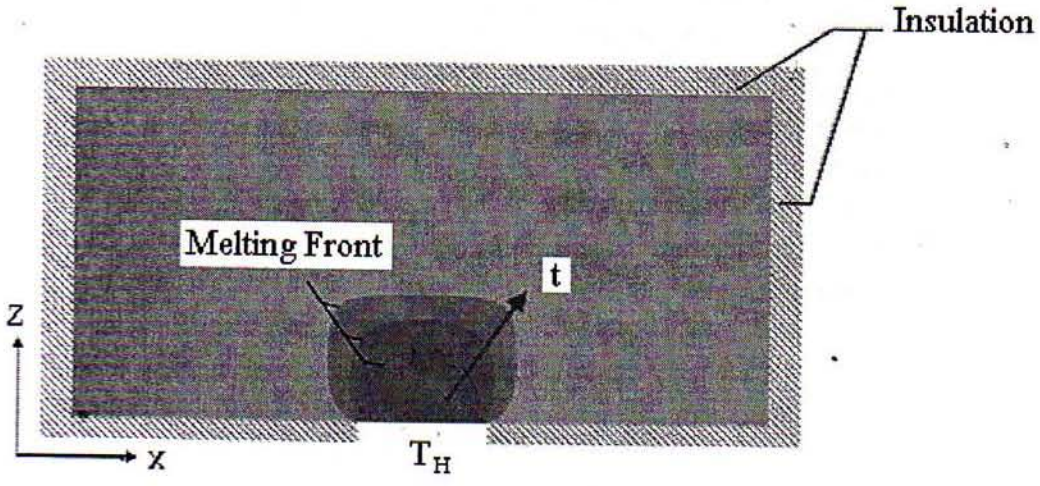

Figure 1. Physical model

The boundary conditions of Eqs. (1) and (2) are (1) the localized heating condition at the bottom horizontal wall (a constant-temperature (T_H) heat source is partially imposed on the bottom wall),

$$x_{cl} \le x_c \le x_{cr}: \quad T = T_H \tag{3}$$

(2) an adiabatic condition (the walls are all insulated),

$$\frac{\partial T}{\partial x} = \frac{\partial T}{\partial z} = 0 \tag{4}$$

and (3) a moving boundary condition. The moving boundary condition (Stefan condition), which is obtained from a consideration of the energy balance at the interface between the unfrozen and frozen layers, provides following equation:

$$\left(\lambda_s \frac{\partial T_s}{\partial z} - \lambda_l \frac{\partial T_l}{\partial z}\right)\left[1 + \left(\frac{\partial z_{\text{mov}}}{\partial x}\right)^2\right] = \rho_s L_s \frac{\partial z_{\text{mov}}}{\partial t} \tag{5}$$

where $\partial z_{\text{mov}}/\partial t$ is the velocity of the fusion front or melting front and L_s is the latent heat of fusion. To avoid changes in the physical dimensions as the melting front progresses, $\rho_s = \rho_l$ will be specified. In this study, λ_l and λ_s denote the thermal conductivity for water and ice, respectively.

3. GRID GENERATION

Generally, two types of structured grid generation are used: the algebraic method, that is, transfinite or multivariate interpolation, and the partial differential equation mapping (PDE mapping) method. Transfinite interpolation provides a relatively easy way of obtaining an initial grid that can be refined and smoothed by other methods, whether algebraic, PDE (this work), or by the variational method. For more complex geometries, such as this work, it is preferable to construct the grid initially by transfinite interpolation and to refine the grid filled in Cartesian coordinates in the interior of a domain by the PDE mapping method.

3.1. Transfinite interpolation

The present method of constructing a two-dimensional boundary-conforming grid for a phase change slab is a direct algebraic approach based on the concept of transfinite interpolation. In this method, no partial differential equations are solved to obtain the curvilinear coordinates, and the same system is used for the entire domain. The algebraic method can be easier to construct than PDE mapping methods and give easier control over grid characteristics such as orthogonality and grid point spacing. However, this method is sometime criticized for allowing discontinuities on the boundary to propagate into the interior and for not generating grids as smooth as those generated by the PDE mapping method. The main idea behind this work, prior to generation of grids by PDE mapping methods, it that it is preferable to obtain first preliminary grids using the algebraic method, that is, the transfinite interpolation method. The combined transfinite interpolation and PDE mapping method is used to achieve a very smooth grids point distribution, and boundary point discontinuities are smoothed out in the interior domain.

For the concept of transfinite interpolation, a significant extension of the original formulation by Gordon and Hall (1973) has made it possible to initially generate a global grid system with geometry specifications only on the outer boundaries of the computational domain and yet obtain a high degree of local control. Moreover, to successfully track the moving boundary front, the grid generation mapping must adapt to large deformations of the interface shape, while maintaining as much orthogonality and smoothness as possible. Owing to the generality of the method, it has been possible to use more advanced mappings than conventional types and thereby improve the overall efficiency of the grid in terms of computational work for a given resolution.

In Fig. 2, the present method of constructing a two-dimensional boundary-conforming grid for a phase change slab is a direct algebraic approach based on the concept of transfinite or multivariate interpolation. It is possible to generate initially global single-plane transformations with geometry specifications only on the outer boundaries of the computational domain.

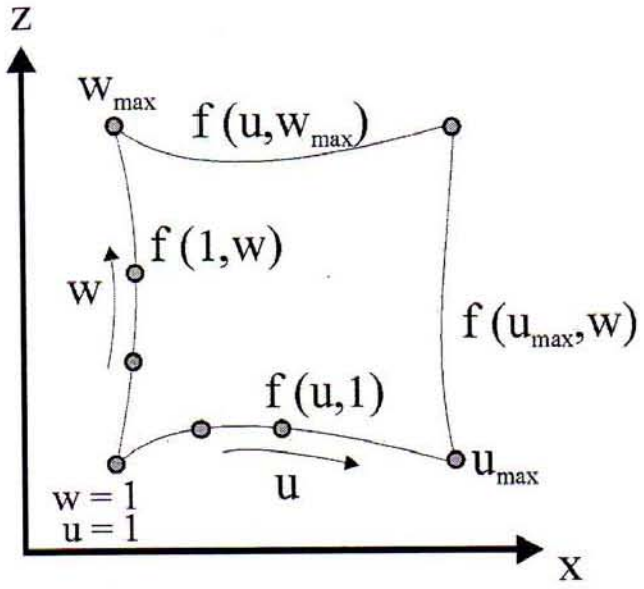

Figure 2. The parametric domain with $f_{(u,w)}$ specified on planes of constant u, w

Let $f(u,w) = (x(u,w), z(u,w))$ denote a vector-valued function of two parameters u, w defined on the region $u_1 \le u \le u_{\max}$, $w_1 \le w \le u_{\max}$. This function is not known throughout the region, only on certain planes (Fig. 2).

The transfinite interpolation procedure then gives the interpolation function $f_{(u,w)}$ by the recursive algorithm:

$$f^{(1)}_{(u,w)} = A_{1(u)} \cdot f_{(1,w)} + A_{2(u)} \cdot f_{(u_{\max},w)}$$
$$f_{(u,w)} = f^{(1)}_{(u,w)} + B_{1(w)} \cdot \left[f_{(u,1)} - f^{(1)}_{(u,1)}\right] + B_{2(w)} \cdot \left[f_{(u,w_{\max})} - f^{(1)}_{(u,w_{\max})}\right] \quad (6)$$

where $A_{1(u)}, A_{2(u)}, B_{1(w)}$ and $B_{2(w)}$ are defined the set of univariate blending functions, which only have to satisfy the conditions

$$A_{1(1)} = 1 \quad A_{1(u_{\max})} = 0$$
$$A_{2(1)} = 0 \quad A_{2(u_{\max})} = 1$$
$$B_{1(1)} = 1 \quad B_{1(w_{\max})} = 0$$
$$B_{2(1)} = 0 \quad B_{2(w_{\max})} = 1$$

Furthermore, the general form in algebraic equations can be defined as

$$A_{1(u)} = \frac{u_{\max} - u}{u_{\max} - 1}, A_{2(u)} = 1 - A_{1(u)}$$
$$B_{1(w)} = \frac{w_{\max} - w}{w_{\max} - 1}, B_{2(w)} = 1 - B_{1(w)} \quad (7)$$

The grid motion defined from a moving boundary motion is modeled using a Stefan equation (Eq. (11)) with a transfinite mapping method. Furthermore, the boundary-fitted grid generation mapping discussed in this section forms the basis for the interface tracking mapping. However, the mapping must now match the interface curve on the interior of the physical domain in addition to fitting the outer physical boundary. In addition, the system must be adaptive since the grid lines must change to follow the deforming interface, while maintaining as much smoothness and orthogonality as possible.

3.2. PDE mapping

In the proposed grid generation mapping, all grids discussed and displayed have been couched in terms of finite difference algorithm applications, with the understanding that whatever nonuniform grid exists in the physical space, there exists a transformation that will recast it as a uniform rectangular grid in the computational space. The finite difference calculations are then made over this uniform grid in the computational space, after which the field results are transferred directly back to the corresponding points in the physical space. The purpose of generating a smooth grid that conforms to physical boundaries of problem is, of course, to solve the partial differential equations specified in the problem by finite difference scheme, capable of handling general nonorthogonal curvilinear coordinates.

Corresponding to Fig. 1, as melting proceeds, a melting front denoted here as z_{mov} is formed. Owing to the existence of this melting front, the frozen and unfrozen domains are irregular and time-dependent. To avoid this difficulty, a curvilinear system of coordinates is used to transform the physical domain into a rectangular region for the computational domain.

It is convenient to introduce a general curvilinear coordinate system, as follows (Anderson, 1995):

$$x = x(\xi,\eta), z = z(\xi,\eta) \quad \text{or}$$
$$\xi = \xi(x,z), \eta = \eta(x,z) \tag{8}$$

The moving boundaries are immobilized in the dimensionless (ξ,η) coordinate for all times. With the details omitted, then, the transformation of Eqs. (1), (2), and (5) can be written, respectively, as

$$\frac{\partial T_l}{\partial t} = \frac{a_l}{J^2}\left(\alpha\frac{\partial^2 T_l}{\partial\xi^2} - 2\beta\frac{\partial^2 T_j}{\partial\xi\partial\eta} + \gamma\frac{\partial^2 T_l}{\partial\eta^2}\right) + \frac{a_l}{J^3}\left[\left(\alpha\frac{\partial^2 x}{\partial\xi^2}\right)\left(z_\xi\frac{\partial T_l}{\partial\eta} - z_\eta\frac{\partial T_l}{\partial\xi}\right) + \alpha\frac{\partial^2 z}{\partial\xi^2} - 2\beta\frac{\partial^2 z}{\partial\xi\partial\eta} + \gamma\frac{\partial^2 z}{\partial\eta^2}\left(-x_\xi\frac{\partial T_l}{\partial\eta}\right)\right] + \frac{1}{J}\left(x_\xi\frac{\partial T_l}{\partial\eta}\right)\frac{dz}{dt} \tag{9}$$

$$\frac{\partial T_s}{\partial t} = \frac{a_s}{J^2}\left(\alpha\frac{\partial^2 T_s}{\partial\xi^2} - 2\beta\frac{\partial^2 T_s}{\partial\xi\partial\eta} + \gamma\frac{\partial^2 T_s}{\partial\eta^2}\right) + \frac{a_s}{J^3}\left[\left(\alpha\frac{\partial^2 x}{\partial\xi^2}\right)\left(z_\xi\frac{\partial T_s}{\partial\eta} - z_\eta\frac{\partial T_s}{\partial\xi}\right) + \alpha\frac{\partial^2 z}{\partial\xi^2} - 2\beta\frac{\partial^2 z}{\partial\xi\partial\eta} + \gamma\frac{\partial^2 z}{\partial\eta^2}\left(-x_\xi\frac{\partial T_s}{\partial\eta}\right)\right] + \frac{1}{J}\left(x_\xi\frac{\partial T_s}{\partial\eta}\right)\frac{dz}{dt} \tag{10}$$

$$\left\{\lambda_s\frac{1}{J}\left(x_\xi\frac{\partial T_s}{\partial\eta}\right) - \lambda_l\frac{1}{J}\left(x_\xi\frac{\partial T_l}{\partial\eta}\right)\right\} \times \left\{1 + \left(\frac{1}{J}\left[z_\eta\frac{\partial z_{\text{mov}}}{\partial\xi} - z_\xi\frac{\partial z_{\text{mov}}}{\partial\eta}\right]\right)^2\right\} = \rho_s L_s\frac{\partial z_{\text{mov}}}{\partial t} \tag{11}$$

where $J = x_\xi \cdot z_\eta - x_\eta \cdot z_\xi$, $\alpha = x_\eta^2 + z_\eta^2$, $\beta = x_\xi \cdot x_\eta + z_\xi \cdot z_\eta$, $\gamma = x_\xi^2 + z_\xi^2$, x_ξ, x_η, z_ξ and z_η denote partial derivatives, J is the Jacobian, β, α, and γ are the geometric factors, and η, ξ are the transformed coordinates. The details of the derivation are briefly provided in the Appendix, with a few examples.

4. SOLUTION METHOD

The transient heat Eqs. (9) and (10) and the Stefan condition (Eq. (11)) are solved using the finite difference method. A system of nonlinear equations results whereby each equation for the internal nodes can be cast into a numerical discretization: Transient Heat Equation for Unfrozen Layer:

$$\begin{aligned}
T_l^{n+1}(k,i) = &\left(\frac{1}{1+\frac{2a_l\Delta t}{J^2(k,i)}\left(\left(\frac{\alpha(k,i)}{\Delta\zeta\Delta\zeta}\right)+\left(\frac{\gamma(k,i)}{\Delta\eta\Delta\eta}\right)\right)}\right) \\
&*\left(T_l^n(k,i)+\frac{a_l\Delta t}{J^2(k,i)} *(\alpha(k,i)(\,T_l^{n-1}(k,i+1)\right. \\
&\left.+\,T_l^{n+1}(k,i-1)\,)/(\Delta\zeta\Delta\zeta)\,)-2\beta(k,i)\right. \\
&\times\left(\left(\frac{T_l^{n-1}(k+1,i+1)-T_l^{n+1}(k-1,i+1)}{2\Delta\eta}\right.\right. \\
&\left.\left.-\frac{T_l^{n-1}(k+1,i-1)-T_l^{n+1}(k-1,i-1)}{2\Delta\zeta}\right)\right)/2\Delta\zeta \\
&+\gamma(k,i)\left(\frac{T_l^{n-1}(k+1,i)+T_l^{n+1}(k-1,i)}{\Delta\eta\Delta\eta}\right)\Bigg)+\frac{a_l\Delta t}{J^3(k,i)} \\
&\times\left(\left(\alpha(k,i)\frac{X(k,i+1)-2X(k,i)+X(k,i-1)}{\Delta\zeta\Delta\zeta}\right)\right. \\
&*\left(\left(\frac{Z(k,i+1)-Z(k,i-1)}{2\Delta\zeta}\right)\right. \\
&*\left(\frac{T_l^{n-1}(k+1,i)-T_l^{n+1}(k-1,i)}{2\Delta\eta}\right) \\
&-\left(\frac{Z(k+1,i)-Z(k-1,i)}{2\Delta\eta}\right) \\
&\left.*\left(\frac{T_l^{n-1}(k,i+1)-T_l^{n+1}(k,i-1)}{2\Delta\zeta}\right)\right)+\alpha(k,i) \\
&\times\left(\frac{Z(k,i+1)-2Z(k,i)+Z(k,i-1)}{\Delta\zeta\Delta\zeta}\right) \\
&-2\beta(k,i)\left(\left(\frac{Z(k+1,i+1)-Z(k-1,i+1)}{2\Delta\eta}\right)\right. \\
&\left.-\left(\frac{Z(k+1,i-1)-Z(k-1,i-1)}{2\Delta\eta}\right)\right)/2\Delta\zeta \\
&+\gamma(k,i)\left(\frac{Z(k+1,i)-2Z(k,i)+Z(k-1,i)}{\Delta\eta\Delta\eta}\right) \\
&*\left(-\frac{(X(k,i+1)-X(k,i-1))}{2\Delta\zeta}\right) \\
&*\left(\frac{T_l^n(k+1,i)-T_l^n(k-1,i)}{2\Delta\eta}\right)+\frac{1}{J(k,i)} \\
&\times\left(\frac{X(k,i+1)-X(k,i-1)}{2\Delta\zeta}\right) \\
&*\left(\frac{T_l^n(k+1,i)-T_l^n(k-1,i)}{2\Delta\eta}\right)*dz(k,i)\Bigg)
\end{aligned} \tag{12}$$

Transient Heat Equation for Frozen Layer:

$$T_s^{n+1}(k,i)=\left(\frac{1}{1+\frac{2a_l\Delta t}{J^2(k,i)}\left(\left(\frac{\alpha(k,i)}{\Delta\zeta\Delta\zeta}\right)+\left(\frac{\gamma(k,i)}{\Delta\eta\Delta\eta}\right)\right)}\right)$$
$$*\left(T_s^n(k,i)+\frac{a_l\Delta t}{J^2(k,i)}*(\alpha(k,i)(T_s^{n-1}(k,i+1)\right.$$
$$\left.+T_s^{n+1}(k,i-1))/(\Delta\zeta\Delta\zeta))-2\beta(k,i)\right.$$
$$\times\left(\left(\frac{T_s^{n-1}(k+1,i+1)-T_s^{n+1}(k-1,i+1)}{2\Delta\eta}\right.\right.$$
$$\left.\left.-\frac{T_s^{n-1}(k+1,i-1)-T_s^{n+1}(k-1,i-1)}{2\Delta\zeta}\right)\right)/2\Delta\zeta$$
$$+\gamma(k,i)\left(\frac{T_s^{n-1}(k+1,i)+T_s^{n+1}(k-1,i)}{\Delta\eta\Delta\eta}\right)\Bigg)$$
$$+\frac{a_l\Delta t}{J^3(k,i)}\left((\alpha(k,i)(X(k,i+1)-2X(k,i)\right.$$
$$\left.+X(k,i-1))/(\Delta\zeta\Delta\zeta))*\left(\left(\frac{Z(k,i+1)-Z(k,i-1)}{2\Delta\zeta}\right)\right.\right.$$
$$*\left(\frac{T_s^{n-1}(k+1,i)-T_s^{n+1}(k-1,i)}{2\Delta\eta}\right)$$
$$-\left(\frac{Z(k+1,i)-Z(k-1,i)}{2\Delta\eta}\right)$$
$$\left.\left.*\left(\frac{T_s^{n-1}(k,i+1)-T_s^{n+1}(k,i-1)}{2\Delta\zeta}\right)\right)+\alpha(k,i)\right.$$
$$\times\left(\frac{Z(k,i+1)-2Z(k,i)+Z(k,i-1)}{\Delta\zeta\Delta\zeta}\right)$$
$$-2\beta(k,i)\left(\left(\frac{Z(k+1,i+1)-Z(k-1,i+1)}{2\Delta\eta}\right)\right.$$
$$\left.-\left(\frac{Z(k+1,i-1)-Z(k-1,i-1)}{2\Delta\eta}\right)\right)/2\Delta\zeta$$
$$+\gamma(k,i)\left(\frac{Z(k+1,i)-2Z(k,i)+Z(k-1,i)}{\Delta\eta\Delta\eta}\right)$$
$$*\left(-\frac{(X(k,i+1)-X(k,i-1))}{2\Delta\zeta}\right)$$
$$*\left(\frac{T_s^n(k+1,i)-T_s^n(k-1,i)}{2\Delta\eta}\right)+\frac{1}{J(k,i)}$$
$$\times\left(\frac{X(k,i+1)-X(k,i-1)}{2\Delta\zeta}\right)$$
$$*\left(\frac{T_s^n(k+1,i)-T_s^n(k-1,i)}{2\Delta\eta}\right)*d\zeta(k,i)\Bigg) \quad (13)$$

Stefan Condition:

$$Z^{n+1}(k,i)=Z^n(k,i)+\frac{\Delta T}{\rho_s L_s}*\left[\left(\frac{\lambda_s}{J(k+1,i)}\right.\right.$$
$$*\left(\frac{X(k+1,i+1)-X(k+1,i-1)}{2\Delta\zeta}\right)$$
$$*\left(\frac{-3T_s(k,i)+4T_s(k+1,i)-T_s(k+2,i)}{2\Delta\eta}\right)$$
$$-\frac{\lambda_l}{J(k-1,i)}*\left(\frac{X(k-1,i+1)-X(k-1,i-1)}{2\Delta\zeta}\right)$$
$$\left.*\left(\frac{3T_l(k,i)-4T_l(k-1,i)+T_l(k-2,i)}{2\Delta\eta}\right)\right)$$
$$*\left(1+\left(\left(\frac{Z^n(k+1,i)-Z^n(k-1,i)}{2\Delta\eta}\right)\right.\right.$$
$$*\left(\frac{Z^n(k+1,i)-Z^n(k-1,i)}{2\Delta\zeta}\right)$$
$$-\left(\frac{Z^n(k,i+1)-Z^n(k,i-1)}{2\Delta\zeta}\right)$$
$$\left.\left.\left.*\left(\frac{Z^n(k,i+1)-Z^n(k,i-1)}{2\Delta\eta}\right)\right)^2\right)\right] \quad (14)$$

The details of computational schemes and the strategy for solving the combined transfinite interpolation functions (Eqs. (6) and (7)) and PDE mapping (Eqs. (12)–(14)) are illustrated in Fig. 3. Here the calculation conditions are as follows: (1) the time step of dt = 0.1 (in seconds) is used for the computation of temperature field and location of melting front; (2) number of grid on entire computational domain N = 100 (width) × 100 (depth); and (3) relative errors in the iteration procedure of 10^{-8} were chosen.

5. EXPERIMENT

The experiment of the melting of the ice slab (with inside dimensions of 10 cm in length (x)× 5 cm in height (z)× 25 cm in depth (y)) subjected to a constant-temperature heat source (T_H = 100°C) is performed. The partial horizontal bottom wall and top wall and the vertical front and back walls are made of acrylic resin. The entire test cell is covered with 8-cm-thick Styrofoam on all sides to minimize the effect of heat losses and condensation of moisture at

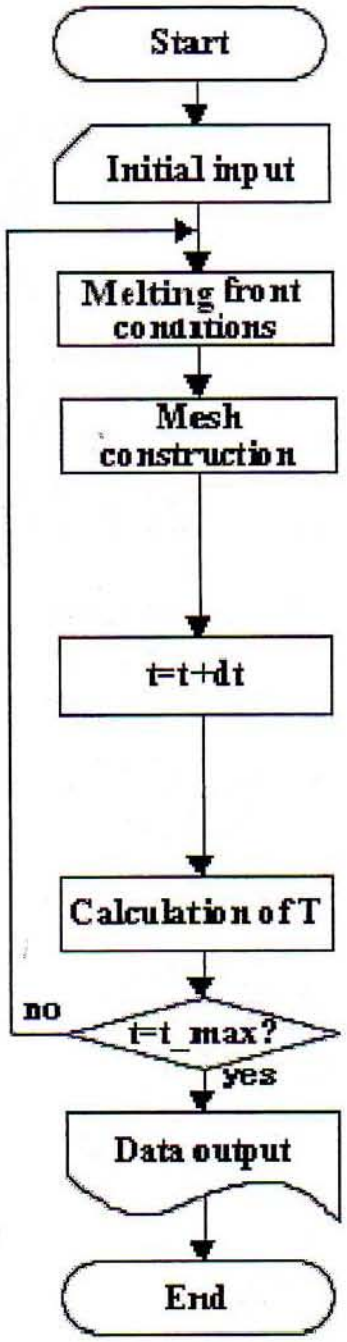

Figure 3. Strategy for calculation

the walls. The partial bottom wall, which serves as a constant temperature heat source, is a multipass heat exchanger. The heat exchanger is connected through a valve system to a constant-temperature bath, where the water is used as the heating medium. The distributions of temperature within the sample are measured using the thermocouples with diameters of 0.015 cm. All thermocouples are set up at 10-mm intervals along the axis of the sample. These thermocouples are connected to a data-logger and computer, through which the temperatures can be measured and stored at preselected time intervals. The positions of the melting front in the sample are determined by interpolating the fusion temperature from the thermocouple reading.

The uncertainty in the results might come from the variations in humidity, room temperature, and human error. The calculated uncertainty associated with temperature is less than 2.65%. The calculated uncertainties in all tests are less than 2.78%.

6. RESULT AND DISCUSSION

6.1. Validation test

To verify the accuracy of the present numerical algorithm, validation was done by performing simulations for a planar melting font in a phase change slab. Initially, a temperature of 0°C is set throughout the slab. Thereafter, the constant-temperature heat source (T_H = 100°C) is imposed on the bottom wall. The calculated front location is based on the thermal properties of ice and water. The results are compared with the analytical solution appearing in the classic book by Carslaw and Jaeger (1959), which is also commonly referred to in literature, for the melting of a phase change slab in the same conditions. Figure 4 clearly shows good agreement of the locations of the melting front. Table 1 again shows good agreement of the values of the melting front between the present solution and the analytical solution. This favorable comparison lends confidence to the accuracy of the numerical results of the present method.

6.2. A melting front tracking grid generation system

To illustrate the efficiency of the grid generation system during the melting of the ice slab (with dimensions of 10 cm (x)× 5 cm (z)) subjected to a constant-temperature heat source, the initial temperature of 0°C is set throughout the slab. Thereafter,

Table 1
Comparison of the melting front obtained in the present study with the analytical solution [a]

Time (s)	Present work	Analytical solution	Difference (%)
120	0.0055	0.0056	1.785
150	0.00618	0.00625	1.12
180	0.0068	0.00686	0.87

[a] See Carslaw and Jaeger (1959)

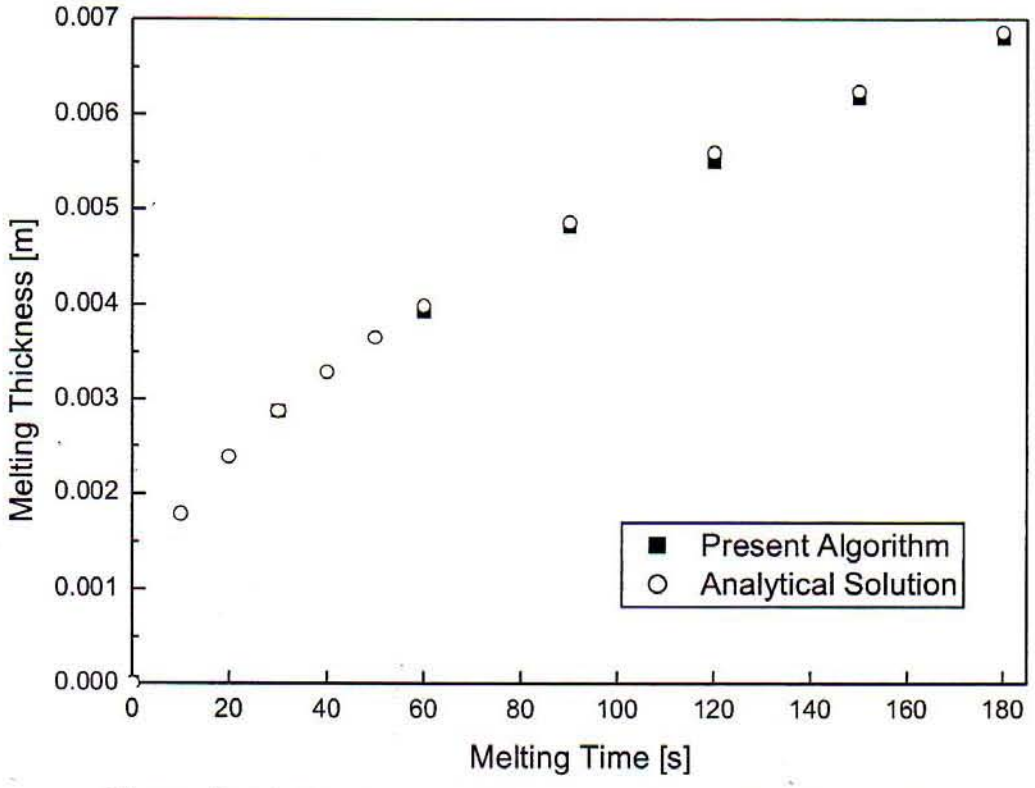

Figure 4. Validation tests for a planar melting font in a phase change slab

the constant-temperature heat source ($T_H = 100°C$) is partially imposed on the bottom wall. To carry out the numerical computations, the computational procedure is presented in Fig. 3 with the thermal properties obtained from Table 2. To initiate numerical simulation, a very thin layer of melt (about 0.1% of the total length of the cavity) with a constant thickness $z_{mov(0)}$ was assumed to be present. This initial condition is obtained from the Stefan solution in the melt and a linear temperature distribution in the ice region. Tests revealed that the influence of $z_{mov(0)}$ could be neglected as $z_{mov(0)}$ was sufficiently small. To check the influence of the numerical grid on the solutions, computations were carried out using 100×50 and 100×100 grids on the entire computational domain, respectively. The results obtained from this study are presented in Fig. 5 in the form of an interface deformation (melting front). It is obvious from the figure that with the present method, the overall interface deformation qualitatively remains the same for two different grids; however, the spreading of the melt in both directions in first case (using 100×50 grids)

Table 2
Thermal properties of the liquid and ice

Property	Unfrozen layer (water)	Frozen layer (ice)
$\rho(kg/m^3)$	999.9	917.0
$a(m^2/s)$	0.131×10^{-6}	1.2×10^{-6}
$\lambda(W/mK)$	0.554	2.2
L (J/kg)		334.9×10^6

is higher than in the second case (using 100 × 100 grids). In addition, it is also evident that the solution had yet to reach a grid-independent state. At this point, it may be mentioned that the main objective of the present article is not to demonstrate the features of the phase change melting problem, but to present a novel numerical approach to solving phase change problems on a moving grid. Hence no further study was carried out to obtain a grid-independent solution, and all subsequent results are presented for the 100 × 100 grid.

The following results (Figs. 6a–6c) show grids that fit curves which are the typical shapes seen during deformation of an interface with respect to elapsed

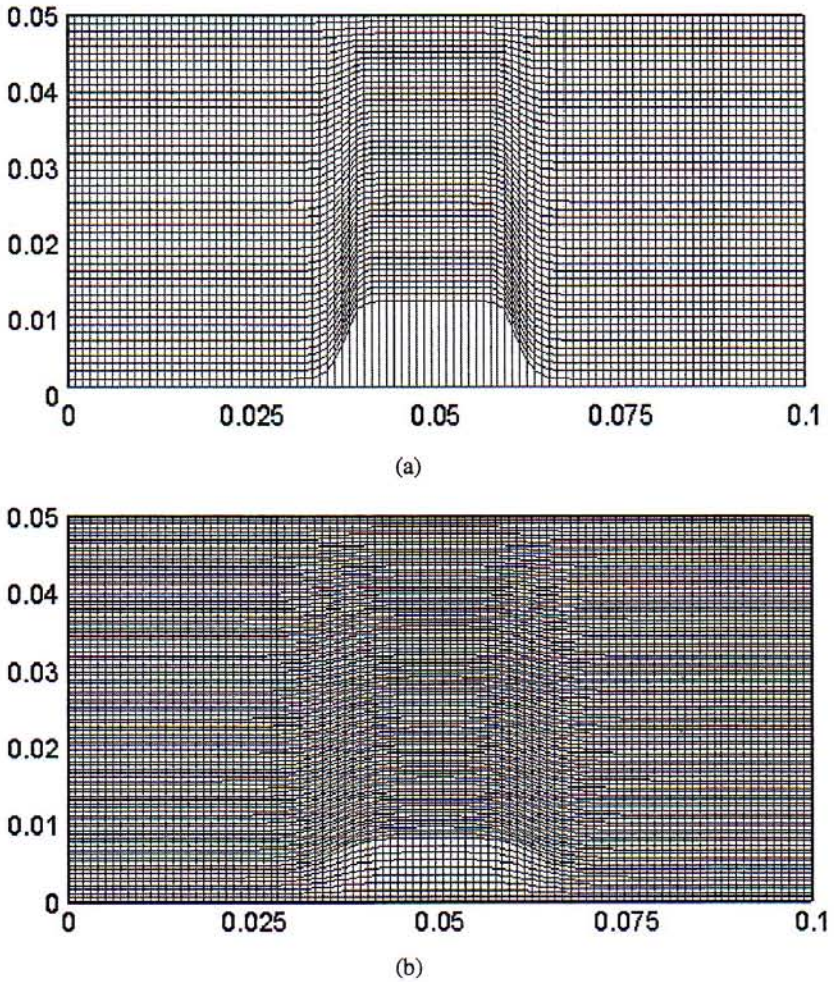

Figure 5. Interface deformation in computational domain with different numerical grids: **a)** 100 × 50 grids and **b)** 100 × 100 grids

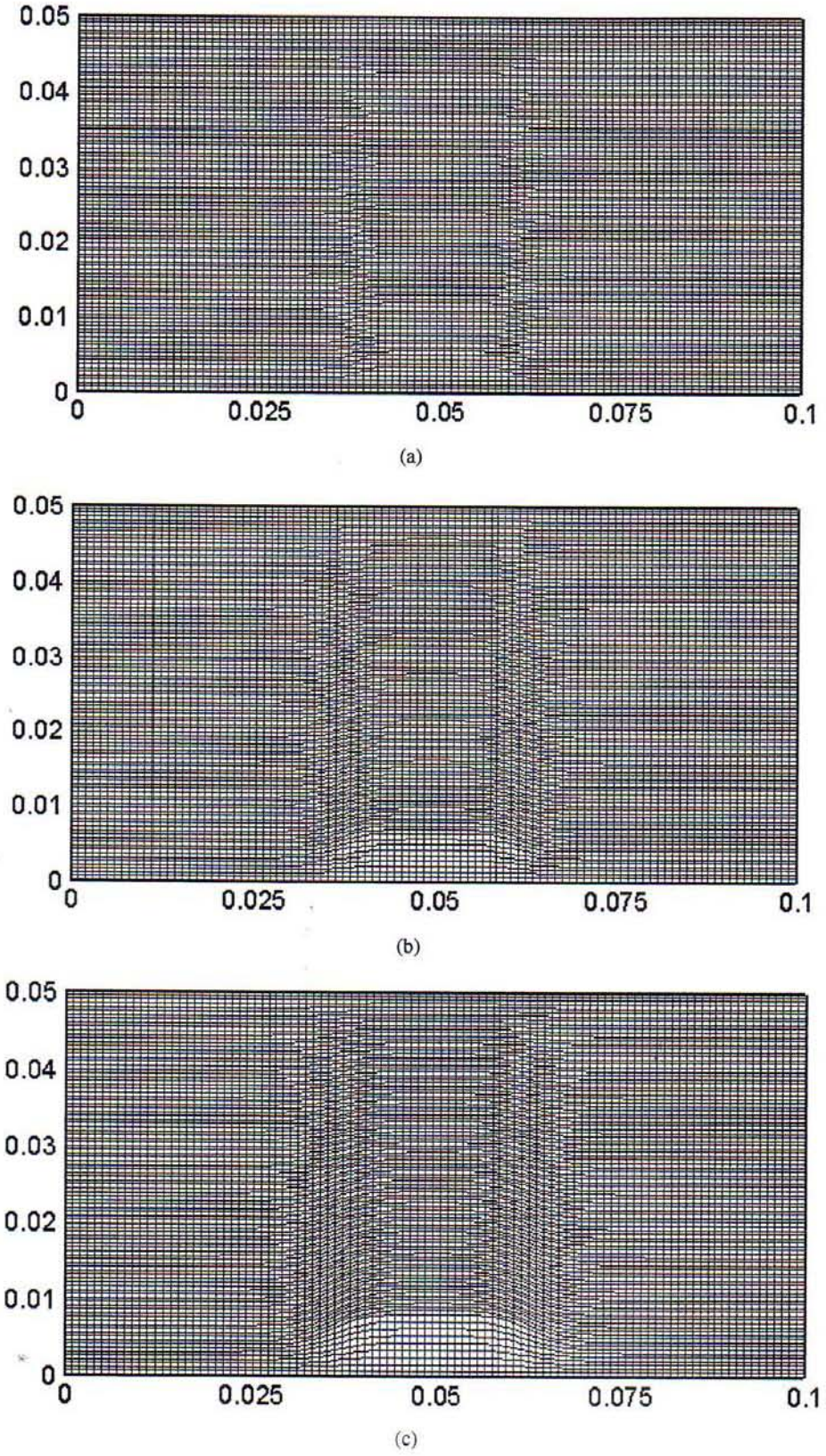

Figure 6. Grid simulating the deformation of an interface: **a)** melting time of 30 s, **b)** melting time of 90 s, and **c)** melting time of 180 s

times. Furthermore, the grids show a significant variation of density and skewness along the interface. It can be seen that the location of the melting front is progressed with respect to elapsed times. During the initial stages of melting, the shape of the interface in each region becomes flatter as the melting front moves farther away from the fixed boundary, indicating principally one-dimensional heat flow. As time progresses, the curve on the interface gradually flattens, indicating the two-dimensional effect.

Figure 7 shows the measured and simulated results of the melting front during the melting of the ice slab (with dimensions of 10 cm (x)× 5 cm (z)) subjected to a constant-temperature heat source. In this comparison, the single constant temperature heat source $T_H = 100°C$ is applied. The observation of the melting front depicted by the figure reveals that the simulated and experimental results are qualitatively consistent, with the value from the experimental data being almost lower than that of the simulated results. The discrepancy may be attributed to heat loss and a nonuniform heating effect along the surface of the supplied load. Numerically, the discrepancy may be attributed to uncertainties in the thermal and physical property data. In addition, the source of the discrepancy may be attributed to a natural convection effect in liquid during the experiment.

The results show that the grid is able to maintain a significant amount of orthogonality and smoothness both within the interior and along the boundary as the grid points redistributed themselves to follow the interface. These results show the efficiency of the present method for the moving boundary problem.

6.3. Melting process

The present work is to couple the grid generation algorithm with the transport equations. The thermal analysis during the melting process will be discussed

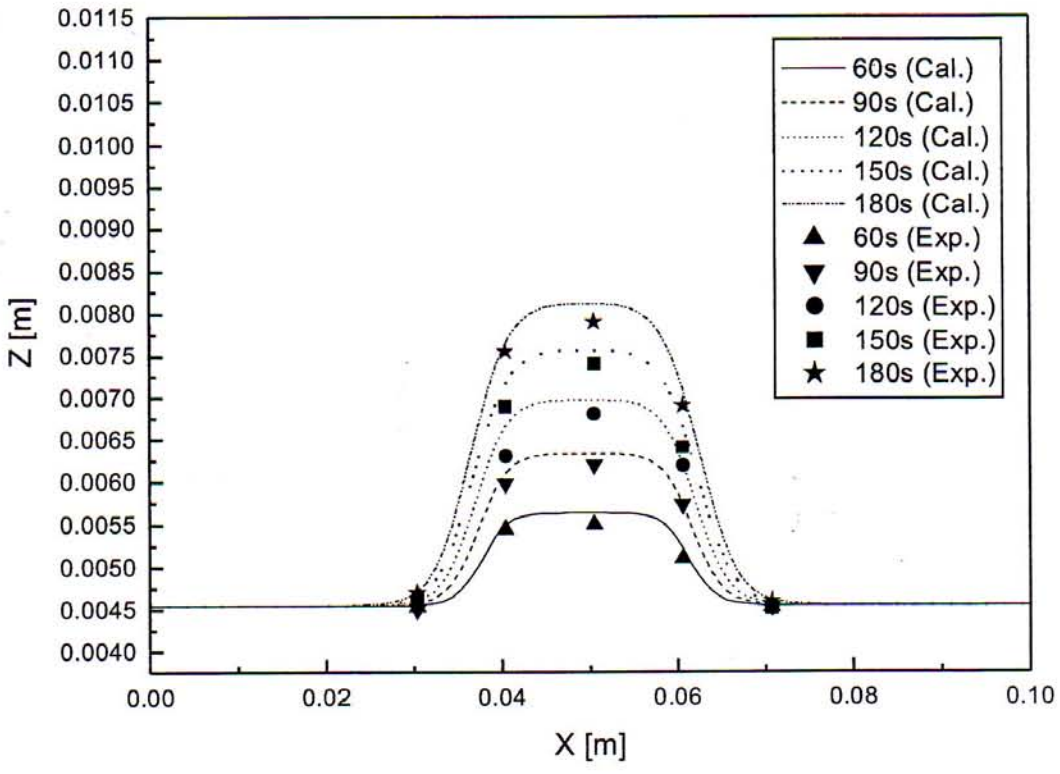

Figure 7. Comparison of experimental data and simulated melting front from the present numerical study

in this section. The simulations of temperature distribution within the ice slab in the vertical plane $(x - z)$ corresponding to a grid simulating the deformation of an interface (Figs. 6a–6c) are shown in Figs. 8a–8c. Since the present work is to couple the grid generation algorithm with the transport equations, the thermal analysis during the melting process will be discussed, as follows. When a constant-temperature heat source ($T_H = 100°C$) is applied during the localized melting process, heat is conducted from the hotter region in the unfrozen layer to the cooler region in the frozen layer. At the initial stages of melting, the melting fronts seem to be square in shape, indicating principally one-dimensional heat flow, as explained for Figs. 6a–6c. Later, the melting fronts gradually exhibit a shape typical for two-dimensional heat conduction–dominated melting. However, as the melting process persists, the melting rate progresses slowly. This is because most of the heat conduction takes place at the leading edge of the unfrozen layer (melt layer), which is located further from the frozen layer. Consequently, a small amount of heat can conduct to the frozen layer due to the melt layer acting as an insulator and causing a slowly melting front to move with respect to elapsed times. Considering the shapes of the melting front with respect to elapsed times, the melt region of the ice slab shows signs of melting, while the outer edge does not display an obvious sign of melting, indicating that the temperature does not exceed 0°C. Nevertheless, at the long stages of the melting process, the spreading of the melt in both the x- and z-directions (semicircular shape) is clearly shown.

The following results refer to the case of the melting of the ice slab with an initial temperature of –10°C. The constant-temperature heat source ($T_H = 100°C$) is partially imposed on the bottom wall. Figures 9a–9c show grids that fit curves that are typical of shapes seen during deformation of an interface with respect to elapsed times. As similarly mentioned in the previous section, the simulated results show the reasonable trends of melting phenomena at specified melting conditions. Nevertheless, the spreading of the melt in this case is lower than that in previous case (Figs. 8a–8c) due to the difference in latent heat at the interface during the melting process.

This study shows the capability of the present method to correctly handle the phase change problem. With further quantitative validation of the present method, this method can be used as a tool for a detailed investigation of this particular melting of the phase change slab at a fundamental level.

7. CONCLUSIONS

This article focuses on establishing a computationally efficient approach for solving the moving boundary heat transfer problem in two-dimensional structured grids, with specific application to a undirectional melting problem. The present work is to couple the grid generation algorithm with the transport equations. The thermal analysis during melting of ice subjected to a constant temperature heat source that partially imposes on the bottom wall is discussed. Preliminary grids are first generated by an algebraic method, based on a transfinite interpolation method, with subsequent refinement using a PDE mapping (parabolic grid generation) method. A preliminary case study indicates successful implementation of the numerical procedure. The algorithm is able to efficiently and accurately predict the evolution of the temperature distribution and deformation of an interface (melting front) with a smooth grid point distribution.

To verify the accuracy of the present numerical study, the present numerical algorithms were validated by performing simulations for a planar melting front in a phase change slab. It shows good agreement with the locations of the moving front. The simulated results from a case study were then compared with experimental results. The observation of the melting front verifies that the simulated and experimental results are qualitatively consistent.

An important application of the present method would be in the field of phase change problems. The next phase, which has already begun, is to couple the grid generation algorithm with the complete transport

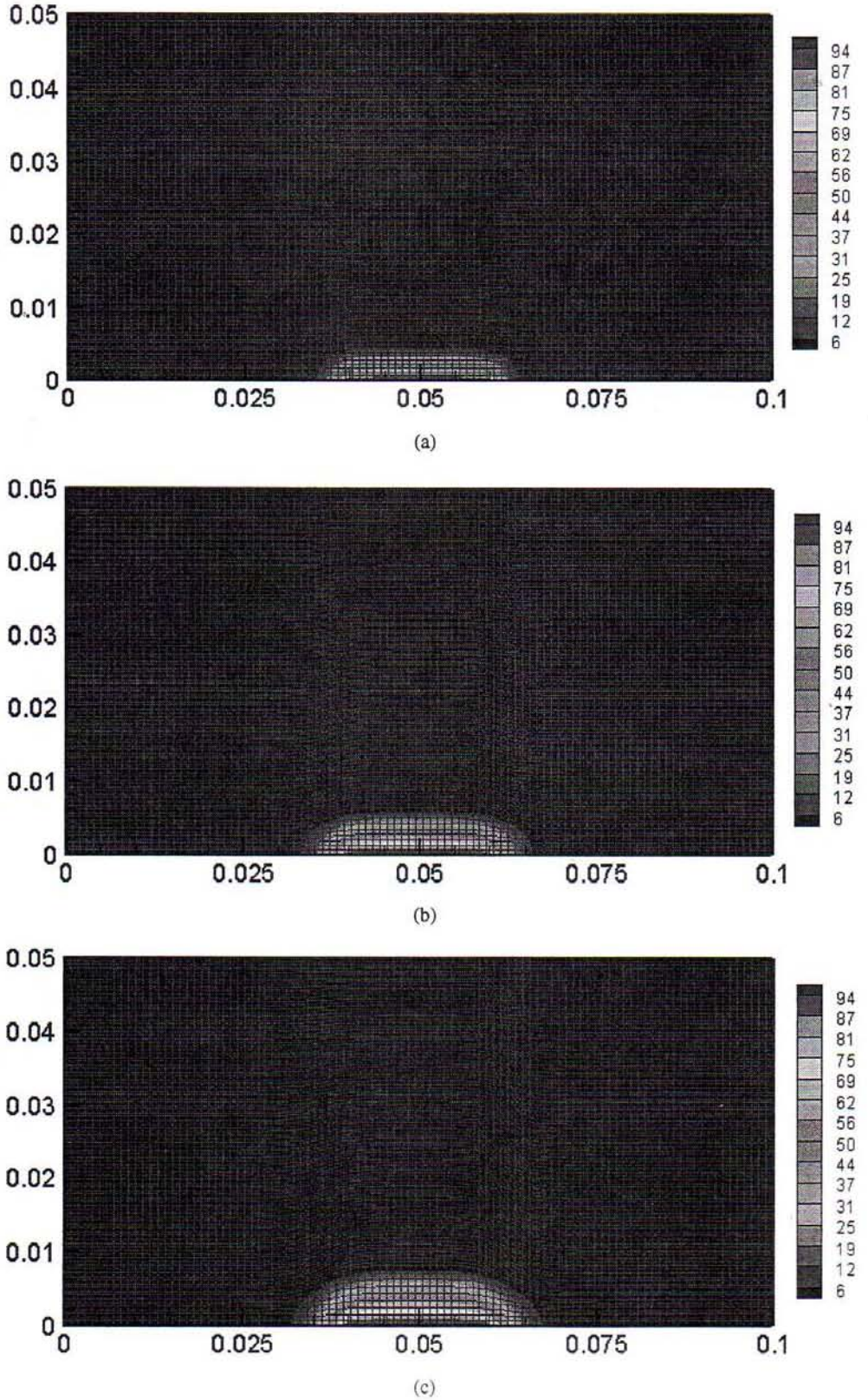

Figure 8. Simulations of temperature distribution (°C): **a**) melting time of 30 s, **b**) melting time of 90 s, and **c**) melting time of 180 s

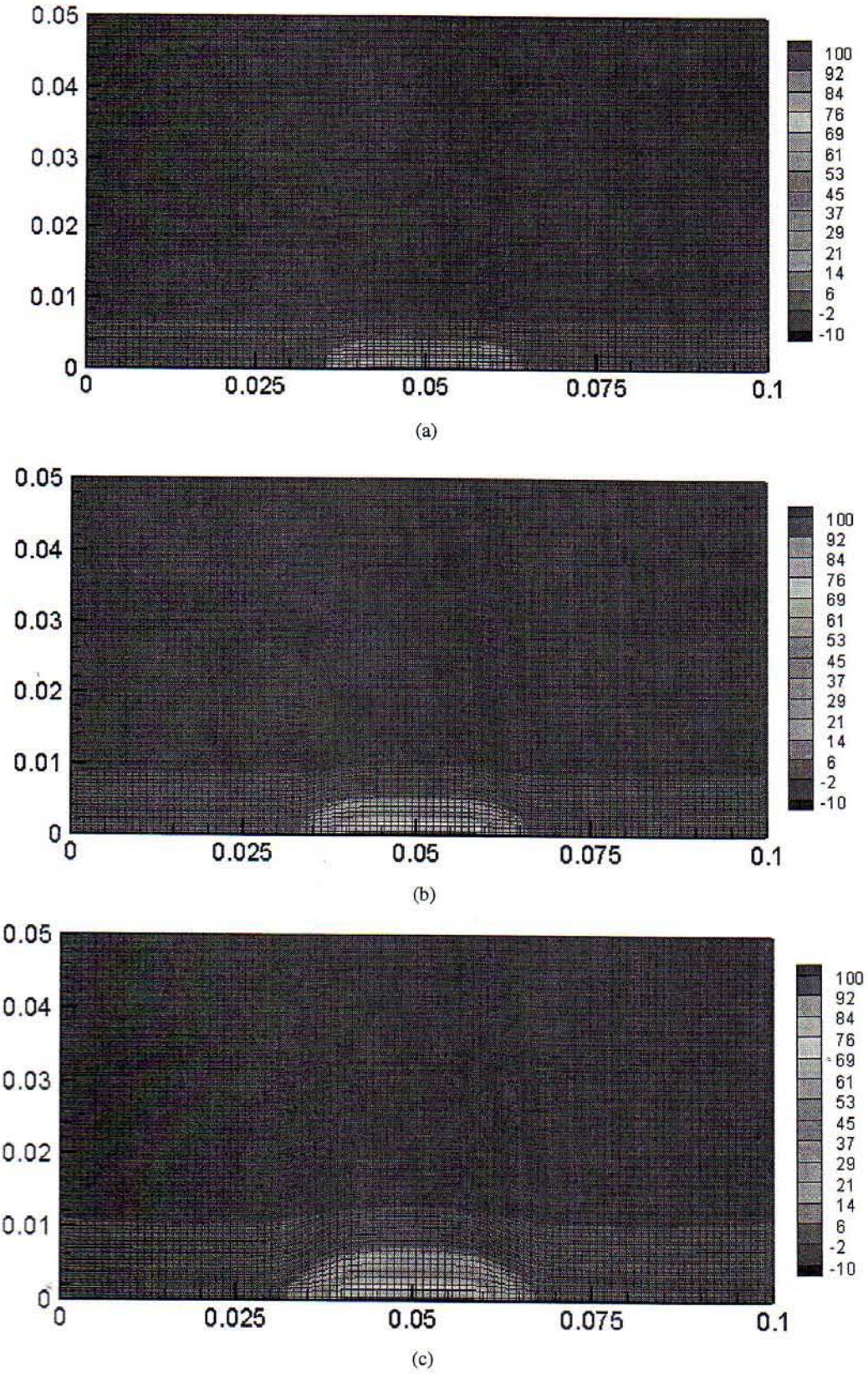

Figure 9. Simulations of temperature distribution (°C): **a)** melting time of 30 s, **b)** melting time of 90 s, and **c)** melting time of 180 s

equations that determine the moving boundary and buoyancy-driven convection in the liquid.

APPENDIX

In this section, we will derive a transformation model of the governing differential equations for use in the numerical calculations. The details are given subsequently.

A.1. General transformation of the first and second derivatives

The first derivative of any parameter can be written as

$$\frac{\partial}{\partial x} = \frac{1}{J} \cdot \left(z_\eta \cdot \frac{\partial}{\partial \xi} - z_\xi \cdot \frac{\partial}{\partial \eta} \right)$$
$$\frac{\partial}{\partial z} = \frac{1}{J} \cdot \left(x_\xi \cdot \frac{\partial}{\partial \eta} - x_\eta \cdot \frac{\partial}{\partial \xi} \right) \tag{A1}$$

Where J is Jacobian, it can be written as

$$J = x_\xi \cdot z_\eta - x_\eta \cdot z_\xi \tag{A2}$$

where

$$x_\xi = \frac{\partial x}{\partial \xi} \tag{A3}$$

Considering the second derivative of any parameter, we will establish the second derivative of the Laplace equation of parameter A, where Eqs. (A1)–(A3) are related:

$$\nabla^2 A = \left(\frac{\partial^2}{\partial x^2} + \frac{\partial^2}{\partial z^2} \right) A = \frac{1}{J^2} \cdot \left(\alpha \cdot \frac{\partial^2 A}{\partial \xi^2} - 2 \cdot \beta \cdot \frac{\partial^2 A}{\partial \xi \partial \eta} + \gamma \cdot \frac{\partial^2 A}{\partial \eta^2} \right) + \frac{1}{J^3} \cdot \left[\left(\alpha \cdot x_{\xi\xi} - 2 \cdot \beta \cdot x_{\xi\eta} + \gamma \cdot x_{\eta\eta} \right) \cdot \left(z_\xi \cdot \frac{\partial A}{\partial \eta} - z_\eta \cdot \frac{\partial A}{\partial \xi} \right) + \left(\alpha \cdot z_{\xi\xi} - 2 \cdot \beta \cdot z_{\xi\eta} + \gamma \cdot z_{\eta\eta} \right) \cdot \left(x_\eta \cdot \frac{\partial A}{\partial \xi} - x_\xi \cdot \frac{\partial A}{\partial \eta} \right) \right] \tag{A4}$$

where

$$\alpha = x_\eta^2 + z_\eta^2$$
$$\beta = x_\xi \cdot x_\eta + z_\xi \cdot z_\eta$$
$$\gamma = x_\xi^2 + z_\xi^2 \tag{A5}$$

x_ξ, x_ξ, z_ξ, and z_η denote partial derivatives, β, α, and γ are the geometric factors, and η, ξ are the transformed coordinates. The related parameter can be defined as

$$x = x(\xi, \eta), \; z = z(\xi, \eta) \text{ or}$$
$$\xi = \xi(x, z), \; \eta = \eta(x, z)$$
$$x = x(\xi), \; z = z(\xi, \eta) \text{ or}$$
$$\xi = \xi(x), \; \eta = \eta(x, z) \tag{A6}$$

$$x_\eta = \frac{\partial x}{\partial \eta} = 0 \quad \text{or} \quad \xi_x = \frac{\partial \xi}{\partial x} = 0$$

Corresponding to Eq. (A6), the first derivative of any parameter (Eq. (A1)) can be rewritten as

$$\frac{\partial}{\partial x} = \frac{1}{J} \cdot \left(z_\eta \cdot \frac{\partial}{\partial \xi} - z_\xi \cdot \frac{\partial}{\partial \eta} \right)$$
$$\frac{\partial}{\partial z} = \frac{1}{J} \cdot \left(x_\xi \cdot \frac{\partial}{\partial \eta} - x_\eta \cdot \frac{\partial}{\partial \xi} \right) \text{ or}$$
$$\frac{\partial}{\partial x} = \frac{1}{J} \cdot \left(z_\eta \cdot \frac{\partial}{\partial \xi} - z_\xi \cdot \frac{\partial}{\partial \eta} \right)$$
$$\frac{\partial}{\partial z} = \frac{1}{J} \cdot \left(x_\xi \cdot \frac{\partial}{\partial \eta} \right) \tag{A7}$$

where

$$J = x_\xi \cdot z_\eta - x_\eta \cdot z_\xi$$
$$J = x_\xi \cdot z_\eta \tag{A8}$$

The second derivative of any parameter (Eqs. (A6)–(A4)) can also be rewritten as

$$\nabla^2 A = \frac{1}{J^2} \cdot \left(\alpha \cdot \frac{\partial^2 A}{\partial \xi^2} - 2 \cdot \beta \cdot \frac{\partial^2 A}{\partial \xi \partial \eta} + \gamma \cdot \frac{\partial^2 A}{\partial \eta^2} \right) + \frac{1}{J^3} \cdot \left[\left(\alpha \cdot x_{\xi\xi} - 2 \cdot \beta \cdot x_{\xi\eta} + \gamma \cdot x_{\eta\eta} \right) \cdot \left(z_\xi \cdot \frac{\partial A}{\partial \eta} - z_\eta \cdot \frac{\partial A}{\partial \xi} \right) + \left(\alpha \cdot z_{\xi\xi} - 2 \cdot \beta \cdot z_{\xi\eta} + \gamma \cdot z_{\eta\eta} \right) \cdot \left(x_\eta \cdot \frac{\partial A}{\partial \xi} - x_\xi \cdot \frac{\partial A}{\partial \eta} \right) \right] \text{ or}$$
$$\nabla^2 A = \frac{1}{J^2} \cdot \left(\alpha \cdot \frac{\partial^2 A}{\partial \xi^2} - 2 \cdot \beta \cdot \frac{\partial^2 A}{\partial \xi \partial \eta} + \gamma \cdot \frac{\partial^2 A}{\partial \eta^2} \right) + \frac{1}{J^3} \cdot \left[\left(\alpha \cdot x_{\xi\xi} \right) \cdot \left(z_\xi \cdot \frac{\partial A}{\partial \eta} - z_\eta \cdot \frac{\partial A}{\partial \xi} \right) + \left(\alpha \cdot z_{\xi\xi} - 2 \cdot \beta \cdot z_{\xi\eta} + \gamma \cdot z_{\eta\eta} \right) \cdot \left(-x_\xi \cdot \frac{\partial A}{\partial \eta} \right) \right] \tag{A9}$$

where

$$\alpha=x_\eta^2+z_\eta^2,\ \beta=x_\xi\cdot x_\eta+z_\xi\cdot z_\eta,\ \gamma=x_\xi^2+z_\xi^2$$

$$\alpha=z_\eta^2,\ \beta=z_\xi\cdot z_\eta,\ \gamma=x_\xi^2+z_\xi^2 \tag{A10}$$

A.2. The transformation of thermal model

After some mathematical manipulations (Eqs. (A7) and (A9) and Eqs. (1), (2), and (5)), a transformation model of the governing differential equations becomes

$$\frac{\partial T_l}{\partial t}=\frac{a_l}{J^2}\left(\alpha\frac{\partial^2 T_l}{\partial\xi^2}-2\beta\frac{\partial^2 T_j}{\partial\xi\partial\eta}+\gamma\frac{\partial^2 T_l}{\partial\eta^2}\right)+\frac{a_l}{J^3}\times\left[\left(\alpha\frac{\partial^2 x}{\partial\xi^2}\right)\left(z_\xi\frac{\partial T_l}{\partial\eta}-z_\eta\frac{\partial T_l}{\partial\xi}\right)+\alpha\frac{\partial^2 z}{\partial\xi^2}-2\beta\frac{\partial^2 z}{\partial\xi\partial\eta}+\gamma\frac{\partial^2 z}{\partial\eta^2}\left(-x_\xi\frac{\partial T_l}{\partial\eta}\right)\right]+\frac{1}{J}\left(x_\xi\frac{\partial T_l}{\partial\eta}\right)\frac{dz}{dt} \tag{A11}$$

$$\frac{\partial T_s}{\partial t}=\frac{a_s}{J^2}\left(\alpha\frac{\partial^2 T_s}{\partial\xi^2}-2\beta\frac{\partial^2 T_s}{\partial\xi\partial\eta}+\gamma\frac{\partial^2 T_s}{\partial\eta^2}\right)+\frac{a_s}{J^3}\times\left[\left(\alpha\frac{\partial^2 x}{\partial\xi^2}\right)\left(z_\xi\frac{\partial T_s}{\partial\eta}-z_\eta\frac{\partial T_s}{\partial\xi}\right)+\alpha\frac{\partial^2 z}{\partial\xi^2}-2\beta\frac{\partial^2 z}{\partial\xi\partial\eta}+\gamma\frac{\partial^2 z}{\partial\eta^2}\left(-x_\xi\frac{\partial T_s}{\partial\eta}\right)\right]+\frac{1}{J}\left(x_\xi\frac{\partial T_s}{\partial\eta}\right)\frac{dz}{dt} \tag{A12}$$

$$\left\{\lambda_s\frac{1}{J}\left(x_\xi\frac{\partial T_s}{\partial\eta}\right)-\lambda_l\frac{1}{J}\left(x_\xi\frac{\partial T_l}{\partial\eta}\right)\right\}\times\left\{1+\left(\frac{1}{J}\left[z_\eta\frac{\partial z_{\mathrm{mov}}}{\partial\xi}-z_\xi\frac{\partial z_{\mathrm{mov}}}{\partial\eta}\right]\right)^2\right\}=\rho_s L_s\frac{\partial z_{\mathrm{mov}}}{\partial t} \tag{A13}$$

8. ACKNOWLEDGMENT

The authors are pleased to acknowledge Thailand Research Fund (TRF) for supporting this research.

REFERENCES

Anderson, J. D., *Computational Fluid Dynamics*, McGraw-Hill, New York, 1995.

Beckett, G., Mackenzie, J. A., and Robertson, M. L., A Moving Mesh Finite Element Method for the Solution of Two-Dimensional Stefan Problems, *J. Comput. Phys.*, vol. **168**, pp. 500–518, 2001.

Beckett, G., Mackenzie, J. A., Ramage, A., and Sloan, D. M., Computational Solution of Two-Dimensional Unsteady PDEs Using Moving Mesh Methods, *J. Comput. Phys.*, vol. **182**, pp. 478–495, 2002.

Cao, W., Huang, W., and Russell, R. D., An r-Adaptive Finite Element Method Based upon Moving Mesh PDEs, *J. Comput. Phys.*, vol. **149**, pp. 221–244, 1999.

Carslaw, H. S, and Jaeger, J. C., *Conduction of Heat in Solids*, 2nd ed., Oxford University Press, New York, 1959.

Chellaiah, S., and Viskanta, R., Freezing of Saturated and Superheated Liquid in Porous Media, *Int. J. Heat Mass Transfer*, vol. **31**, pp. 321–330, 1988.

Cook, W. A., Body Oriented Coordinates for Generating 3-Dimensional Meshes, *Int. J. Numer. Methods Eng.*, vol. **8**, pp. 27–43, 1974.

Coons, S. A., Surfaces for Computer-Aided Design of Space Forms, Project MAC, Tech. Rep. MAC-TR 44, Massachusetts Institute of Technology, Cambridge, 1967.

Ettouney, H. M., and Brown, R. A., Finite-Element Methods for Steady Solidification Problems, *J. Comput. Phys.*, vol. **49**, pp. 118–150, 1983.

Eriksson, L. E., Generation of Boundary-Conforming Grid Around Wing-Body Configurations Using Transfinite Interpolation, *AIAA J.*, vol. **20**, pp. 1313-1320, 1982.

Fachinotti, V. D., Cardona, A., and Huespe, A. E., A Fast Convergent and Accurate Temperature Model for Phase Change Heat Conduction, *Int. J. Heat Mass Transfer*, vol. **44**, pp. 1863–1884, 1999.

Frivik, P. E., and Comini, G., Seepage and Heat Flow in Soil Freezing, *ASME J. Heat Transfer*, vol. **104**, pp. 323–328, 1982.

Gong, Z.-X., and Mujumdar, A. S., Flow and Heat Transfer in Convection-Dominated Melting in a Rectangular Cavity Heated from Below, *Int. J. Heat Mass Transfer*, vol. **41**, pp. 2573–2580, 1998.

Gordon, W. J., and Hall, C. A., Construction of Curvilinear Coordinate Systems and Applications to Mesh Generation, *Int. J. Numer. Methods Eng.*, vol. **7**, pp. 461–477, 1973.

Gupta, S. C., A Moving Grid Numerical Scheme for Multi-dimensional Solidification with Transition Temperature Range, *Comput. Methods Appl. Mech. Eng.*, vol. **189**, pp. 525–544, 2000.

Landua, H. G., Heat Conduction in a Melting Solid, *Q. Appl. Math.*, vol. **8**, pp. 81–94, 1950.

Mackenzie, J. A., and Robertson, M. L., The Numerical Solution of One-Dimensional Phase Change Problems Using an Adaptive Moving Mesh Method, *J. Comput. Phys.*, vol. **161**, pp. 537–557, 2000.

Morgan, K., Lewis, R. W., and Zienkiewicz, O. C., An Improved Algorithm for Heat Conduction Problems with Phase Change, *Int. J. Numer. Methods Eng.*, vol. **12**, pp. 1191–1195, 1978.

Murray, W. D., and Landis, F., Numerical and Machine Solutions of Transient Heat Conduction Problem Involving Melting or Freezing, *ASME J. Heat Transfer*, vol. **81**, pp. 106–112, 1959.

Nedjar, B., An Enthalpy-Based Finite Element Method for Non-linear Heat Problems Involving Phase Change, *Comput. Struct.*, vol. **80**, pp. 9–21, 2002.

Pardo, E., and Weckman, D. C., A Fixed Grid Finite Element Technique for Modeling Phase Change in Steady State Conduction-Advection Problems, *Int. J. Numer. Methods Eng.*, vol. **29**, pp. 969–984, 1990.

Rattanadecho, P., Experimental and Numerical Study of Solidification Process in Unsaturated Granular Packed Bed, *AIAA J. Thermophys. Heat Transfer*, vol. **18**, pp. 87–93, 2004a.

Rattanadecho, P., The Theoretical and Experimental Investigation of Microwave Thawing of Frozen Layer Using Microwave Oven (Effects of Layered Configurations and Layered Thickness), *Int. J. Heat Mass Transfer*, vol. **47**, pp. 937–945, 2004b.

Tamma, K. K., and Namburu, R. R., Recent Advances, Trends and New Perspectives via Enthalpy-Based Finite Element Formulations for Applications to Solidification Problems, *Int. J. Numer. Methods Eng.*, vol. **30**, pp. 803–820, 1990.

Tenchev, R. T., Mackenzie, J. A., Scanlon, T. J., and Stickland, M. T., Finite Element Moving Mesh Analysis of Phase Change Problems with Natural Convection, *Int. J. Heat Fluid Flow*, vol. **26**, pp. 597–612, 2005.

Voller, V., and Cross, M., Accurate Solutions of Moving Boundary Problems Using the Enthalpy Method, *Int. J. Heat Mass Transfer*, vol. **24**, pp. 545–556, 1981.

Voller, V. R., Swaminathan, C. R., and Thomas, B. G., Fixed Grid Techniques for Phase Change Problems: A Review, *Int. J. Numer. Methods Eng.*, vol. **30**, pp. 875–898, 1990.

Weaver J. A., and Viskanta R., Freezing of Liquid-Saturated Porous Media, *ASME J. Heat Transfer*, **108**, pp. 654–659, 1986.